INTERNATIONAL JOURNAL FOR NUMERICAL METHODS IN FLUIDS
Int. J. Numer. Meth. Fluids 2008; **58**:945–967
Published online 17 March 2008 in Wiley InterScience (www.interscience.wiley.com). DOI: 10.1002/fld.1778

A finite-volume particle method for conservation laws on moving domains

D. Teleaga[1] and J. Struckmeier[2,*,†]

[1]*Department of Mathematics, Technical University of Darmstadt, Darmstadt, Germany*
[2]*Department of Mathematics, University of Hamburg, Hamburg, Germany*

SUMMARY

The paper deals with the finite-volume particle method (FVPM), a relatively new method for solving hyperbolic systems of conservation laws. A general formulation of the method for bounded and moving domains is presented. Furthermore, an approximation property of the reconstruction formula is proved. Then, based on a two-dimensional test problem posed on a moving domain, a special Ansatz for the movement of the particles is proposed. The obtained numerical results indicate that this method is well suited for such problems, and thus a first step to apply the FVPM to real industrial problems involving free boundaries or fluid–structure interaction is taken. Finally, we perform a numerical convergence study for a shock tube problem and a simple linear advection equation. Copyright © 2008 John Wiley & Sons, Ltd.

Received 16 February 2007; Revised 29 December 2007; Accepted 2 January 2008

KEY WORDS: hyperbolic systems; meshless methods; finite-volume schemes; non-Lagrangian methods

1. INTRODUCTION

The finite-volume particle method (FVPM) is a relatively new meshless method for solving hyperbolic systems of conservation laws, firstly developed in 1998 by Hietel *et al.* [1]. There the FVPM is formulated for a system of conservation laws in the spatial domain $\Omega = \mathbb{R}^d$ and shown to be conservative. Later, Junk and Struckmeier [2] proposed a more stable discretization and proved a Lax–Wendroff-type consistency result for scalar conservation laws in $\Omega = \mathbb{R}$. The motivation to develop this new scheme was to unify the advantages of finite-volume methods (FVMs) and particle methods in one scheme. The FVPM combines the generic features of a finite-volume scheme and

*Correspondence to: J. Struckmeier, Department of Mathematics, University of Hamburg, Hamburg, Germany.
†E-mail: struckmeier@math.uni-hamburg.de

Contract/grant sponsor: DFG-Stipendium

a particle method, namely the concept of a numerical flux function and the flow description using moving particles.

This method was also the subject of concern in [3–10]. The extension of the projection technique for incompressible flows to the FVPM is done in [4, 5]. Isotropic and anisotropic adaptive strategies are investigated in [7]. Moreover, a coupling approach between the classical FVM and the FVPM is proposed in [10]. In [6] an application of the FVPM to a problem with moving boundary in one space dimension is given. Thus, the scheme was mainly tested on one- and two-dimensional problems posed on fixed domains, problems where also the mesh-based methods work. However, being a mesh-free method, the FVPM is intended for problems where a mesh-based method may fail, such as problems with moving or free boundaries or fluid–structure interaction problems.

Here we wish to take a step forward in applying the FVPM to real industrial problems involving free boundaries or fluid–structure interaction. Therefore, after deriving the FVPM on fixed and bounded domains, we formulate it on moving domains and apply it to a two-dimensional test problem with moving boundary. With this example, we also wish to exploit an advantage of the FVPM over SPH methods, namely the fact that in FVPM the particles may move in a non-Lagrangian way.

We end up with a numerical convergence study of the FVPM for a shock tube problem and a simple linear advection equation. For these cases our FVPM will not be competitive with grid-based finite-volume schemes, which we even observe in the results of the estimated order of convergence (EOC).

1.1. Derivation of FVPM on fixed domains

Here we follow the derivation made in [2], but for a system of conservation laws on a bounded domain $\Omega \subset R^d$.

We consider conservation laws expressed in the form

$$\partial_t \mathbf{u} + \nabla \cdot \mathscr{F}(\mathbf{u}) = \mathbf{0} \quad \forall \mathbf{x} \in \Omega \subset R^d, \ \ t > 0 \tag{1}$$

with initial conditions $\mathbf{u}(\mathbf{x}, 0) = \mathbf{u}_0(\mathbf{x})$, $\forall \mathbf{x} \in \Omega$, and with suitable boundary conditions, where $\Omega \subset R^d$ is a bounded domain, $\mathbf{u}(\mathbf{x}, t) \in R^m$, $m > 0$ denotes the vector of conservative quantities, and $\mathscr{F}(\mathbf{u}(\mathbf{x}, t))$ denotes the flux function of the conservation law.

A natural approach to discretize conservation laws is to evaluate the weak formulation of (1) with a discrete set of test functions ψ_i, $i = 1, \ldots, N$. In classical FVMs [11], the test functions are taken as the characteristic functions $I_{\Omega_i}(\mathbf{x})$ of the control volumes Ω_i. The discrete quantities are obtained from cell averages. Note that the characteristic functions form a partition of unity, i.e. $\sum_{i=1}^{N} I_{\Omega_i}(\mathbf{x}) = 1, \forall \mathbf{x} \in \Omega$.

A similar approach is used in the following, but we introduce a different set of test functions. Since we wish to derive a mesh-free method, we should not make use of a mesh. Therefore, the conservative variables are approximated at each time step by a finite set of particles located in the spatial domain Ω. From this point of view, the FVPM is a particle method with particle positions $\mathbf{x}_i(t)$, which may be irregularly spaced and moving in time. To each position $\mathbf{x}_i(t)$, we associate a function $\psi_i(\mathbf{x}, t)$, which we call *a particle*. As in the finite-volume approach, let $\{\psi_i : i = 1, \ldots, N\}$ be a partition of unity, but the supports of the functions should overlap. More exactly, we assume that the particles are smooth functions localized around the particle positions $\mathbf{x}_i(t)$ and

DOI: 10.1002/fld

satisfy

$$\sum_{i=1}^{N} \psi_i(\mathbf{x},t)=1 \quad \forall \mathbf{x}\in\Omega,\ \ t\geqslant 0 \tag{2}$$

We construct this partition of unity as follows:

Taking a Lipschitz-continuous function $W: R\to R_+$ with compact support (otherwise one has to consider long-range interactions between particles), we define

$$\psi_i(\mathbf{x},t)=\frac{W_i(\mathbf{x},t)}{\sigma(\mathbf{x},t)} \tag{3}$$

where $\sigma(\mathbf{x},t)=\sum_{i=1}^{N} W_i(\mathbf{x},t)$ and $W_i(\mathbf{x},t)=W(\mathbf{x}-\mathbf{x}_i(t));\ i=1,\ldots,N$. Such a partition of unity used in the FVPM in the one-dimensional case is shown in Figure 1. It is computed using the function W, also called *smoothing kernel*:

$$W(x)=\begin{cases} (x+h)^2, & x\in\left[-h,-\dfrac{h}{2}\right) \\ -x^2+\dfrac{h^2}{2}, & x\in\left[-\dfrac{h}{2},\dfrac{h}{2}\right) \\ (x-h)^2, & x\in\left[\dfrac{h}{2},h\right) \\ 0 & \text{otherwise} \end{cases} \tag{4}$$

where the parameter $h>0$ is the so-called *smoothing length*.

Now, we test the conservation law (1) against the new set of test functions $\psi_i(\mathbf{x},t)$, i.e. we consider the weak form given by

$$\int_\Omega (\partial_t \mathbf{u}+\nabla\cdot\mathscr{F}(\mathbf{u}))\psi_i(\mathbf{x},t)\,\mathrm{d}\mathbf{x}=0, \quad i=1,\ldots,N \tag{5}$$

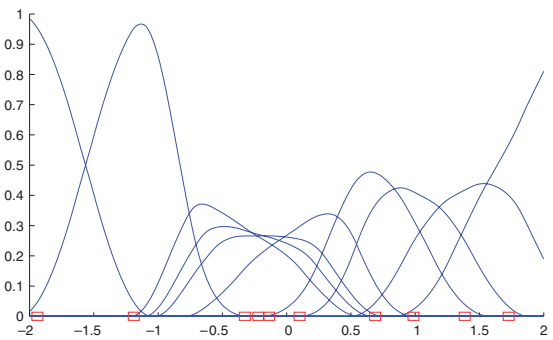

Figure 1. A partition of unity used in the FVPM: on the x-axis are indicated the particle positions x_i and around each x_i is plotted the function ψ_i.

DOI: 10.1002/fld

which yields the equations

$$\frac{\mathrm{d}}{\mathrm{d}t}\int_\Omega \mathbf{u}\psi_i\,\mathrm{d}\mathbf{x}=\int_\Omega (\mathscr{F}(\mathbf{u})\cdot\nabla\psi_i+\mathbf{u}\,\partial_t\psi_i)\,\mathrm{d}\mathbf{x}-\int_{\partial\Omega}\psi_i\mathscr{F}(\mathbf{u})\cdot\mathbf{n}\,\mathrm{d}\sigma \tag{6}$$

Note that the boundary term appears only for particles i that are close to the boundary, i.e. $\operatorname{supp}\psi_i\cap\partial\Omega\neq 0$.

Similar to FVMs, one associates with each particle a local average $\mathbf{u}_i(t)$ through the relation

$$\mathbf{u}_i(t)=\frac{1}{V_i(t)}\int_\Omega \mathbf{u}(\mathbf{x},t)\psi_i(\mathbf{x},t)\,\mathrm{d}\mathbf{x} \tag{7}$$

where $V_i(t)$ is the time-dependent volume of a particle i given by

$$V_i(t)=\int_\Omega \psi_i(\mathbf{x},t)\,\mathrm{d}\mathbf{x} \tag{8}$$

Using definition (3), one may obtain [1, 2] the following equations from (6):

$$\frac{\mathrm{d}}{\mathrm{d}t}(V_i\mathbf{u}_i)=\sum_{j=1}^{N}\int_\Omega((\mathscr{F}(\mathbf{u})-\mathbf{u}\dot{\mathbf{x}}_i)\mathbf{\Gamma}_{ji}-(\mathscr{F}(\mathbf{u})-\mathbf{u}\dot{\mathbf{x}}_j)\mathbf{\Gamma}_{ij})\,\mathrm{d}\mathbf{x}-\mathscr{B}_i \tag{9}$$

where $\mathbf{\Gamma}_{ij}$ is a function localized on the intersection of the supports of particle i and particle j given by

$$\mathbf{\Gamma}_{ij}(\mathbf{x},t)=\frac{\psi_i(\mathbf{x},t)}{\sigma(\mathbf{x},t)}\nabla W_j(\mathbf{x},t)\quad\forall i,j=1,\ldots,N \tag{10}$$

and $\mathscr{B}_i=\int_{\partial\Omega}\psi_i\mathscr{F}(\mathbf{u})\cdot\mathbf{n}\,\mathrm{d}\sigma$ denotes the boundary term. The treatment of a boundary particle i consists of two parts: first we cut off that part of its support, which lies outside the domain Ω and then we discretize the corresponding boundary term such that the given boundary conditions are satisfied. In the case of inlet or outlet boundary conditions, we have

$$\int_{\partial\Omega}\psi_i\mathscr{F}(\mathbf{u})\cdot\mathbf{n}\,\mathrm{d}\sigma\approx\mathscr{F}(\mathbf{u}_i^*)\int_{\partial\Omega}\psi_i\mathbf{n}\,\mathrm{d}\sigma=-\mathscr{F}(\mathbf{u}_i^*)\sum_{j\in N(i)}\boldsymbol{\beta}_{ij} \tag{11}$$

where we used relation (23) and $\mathbf{u}_i^*$ approximates $\mathbf{u}$ on $\Omega_i\cap\partial\Omega$. At a solid wall boundary, the normal velocity of a compressible flow is zero. As a consequence, all convective flux components through the solid wall will vanish in the computation of the flux terms and we obtain

$$\int_{\partial\Omega}\psi_i\mathscr{F}(\mathbf{u})\cdot\mathbf{n}\,\mathrm{d}\sigma\approx\begin{pmatrix}0\\-p_i\sum_j\boldsymbol{\beta}_{ij}\\0\end{pmatrix} \tag{12}$$

For more details, see [9].

For abbreviation, we introduce the modified flux

$$\mathscr{G}(t,\dot{\mathbf{x}},\mathbf{u})=\mathscr{F}(\mathbf{u})-\mathbf{u}\cdot\dot{\mathbf{x}} \tag{13}$$

DOI: 10.1002/fld

where the particle movement $\dot{\mathbf{x}}$ is given by $\dot{\mathbf{x}}(t)=\mathbf{a}(\mathbf{x},t)$, $\mathbf{a}(\mathbf{x},t)\in C^0(R_+,C^1(R^d))$ being a given velocity field. The modified flux $\mathscr{G}$ consists of the flux of the given conservation law, as well of a contribution $\mathbf{u}\cdot\mathbf{a}$ due to the particle movement with velocity $\mathbf{a}$.

Remark
The velocity $\mathbf{a}$ of the particles is not a Lagrangian-type velocity, but an almost arbitrarily chosen vector function. The vector $\mathbf{a}$ should be in such a way that during the movement of the particles their supports always cover the domain completely.

Now, assuming that $\mathbf{u}$ varies only slightly around a certain, but fixed $\bar{\mathbf{u}}$ on the intersection of the supports of ψ_i and ψ_j, and that $\dot{\mathbf{x}}_i\approx\dot{\mathbf{x}}_j:=\bar{\dot{\mathbf{x}}}$, with, e.g. $\bar{\dot{\mathbf{x}}}=(\dot{\mathbf{x}}_i+\dot{\mathbf{x}}_j)/2$, we have

$$\frac{\mathrm{d}}{\mathrm{d}t}(V_i\mathbf{u}_i)\approx-\sum_{j=1}^{N}(\mathscr{F}(\bar{\mathbf{u}})-\bar{\mathbf{u}}\bar{\dot{\mathbf{x}}})\int_\Omega(\boldsymbol{\Gamma}_{ij}-\boldsymbol{\Gamma}_{ji})\,\mathrm{d}\mathbf{x}-\mathscr{B}_i$$

$$=-\sum_{j=1}^{N}|\boldsymbol{\beta}_{ij}|(\mathscr{F}(\bar{\mathbf{u}})-\bar{\mathbf{u}}\bar{\dot{\mathbf{x}}})\cdot\mathbf{n}_{ij}-\mathscr{B}_i$$

where

$$\boldsymbol{\beta}_{ij}(t)=\boldsymbol{\gamma}_{ij}(t)-\boldsymbol{\gamma}_{ji}(t)\quad\text{and}\quad\mathbf{n}_{ij}=\frac{\boldsymbol{\beta}_{ij}}{|\boldsymbol{\beta}_{ij}|}\tag{14}$$

with $\boldsymbol{\gamma}_{ij}(t)=\int_\Omega\boldsymbol{\Gamma}_{ij}(\mathbf{x},t)\,\mathrm{d}\mathbf{x}$.

The flux is approximated in terms of the discrete values with the help of a numerical flux function $\mathbf{g}_{ij}=\mathbf{g}(t,\mathbf{x}_i,\mathbf{u}_i,\mathbf{x}_j,\mathbf{u}_j,\mathbf{n}_{ij})$ of the modified flux function $\mathscr{G}(t,\dot{\mathbf{x}},\mathbf{u})$, i.e. we use the approximation

$$(\mathscr{F}(\bar{\mathbf{u}})-\bar{\mathbf{u}}\bar{\dot{\mathbf{x}}})\cdot\mathbf{n}_{ij}\approx\mathbf{g}_{ij}$$

Remark
The numerical flux function $\mathbf{g}$ can be any numerical flux function used in FVM, but it has to be consistent with the modified flux function $\mathscr{G}$, not with $\mathscr{F}$. In the case considered above, if $\dot{\mathbf{x}}(t)=\mathbf{a}(\mathbf{x},t)$, i.e. $\dot{\mathbf{x}}(t)\neq\mathbf{a}(\mathbf{x},t,\mathbf{u})$, one can easily modify a numerical flux function consistent with $\mathscr{F}$ to generate a flux function consistent with $\mathscr{G}(t,\dot{\mathbf{x}},\mathbf{u})=\mathscr{F}(\mathbf{u})-\mathbf{u}\cdot\dot{\mathbf{x}}$.

One ends up with the following system of ordinary differential equations (ODEs):

$$\frac{\mathrm{d}}{\mathrm{d}t}(V_i\mathbf{u}_i)=-\sum_{j=1}^{N}|\boldsymbol{\beta}_{ij}|\mathbf{g}_{ij}-\mathscr{B}_i\tag{15}$$

with the initial condition

$$\mathbf{u}_i(0)=\frac{1}{V_i(0)}\int_\Omega\mathbf{u}_0(\mathbf{x})\psi_i(\mathbf{x},0)\,\mathrm{d}\mathbf{x}\tag{16}$$

Using an explicit Euler discretization of the time derivative, the resulting scheme has a structure similar to that of an FVM scheme, namely

$$V_i^{n+1}\mathbf{u}_i^{n+1}=V_i^n\mathbf{u}_i^n-\Delta t\sum_{j\in N(i)}|\boldsymbol{\beta}_{ij}^n|\mathbf{g}_{ij}^n-\mathscr{B}_i\tag{17}$$

DOI: 10.1002/fld

with $\mathbf{u}_i^0 = 1/V_i^0 \int_\Omega \mathbf{u}_0(\mathbf{x})\psi_i(\mathbf{x},0)\,\mathrm{d}\mathbf{x}$. The set $N(i)$ denotes the neighbours of a particle i, i.e. the particles j with the property that $\operatorname{supp}\psi_j \cap \operatorname{supp}\psi_i \neq \emptyset$.

A natural reconstruction of a function from the discrete values is given by

$$\tilde{\mathbf{u}}(\mathbf{x},t) = \sum_{i=1}^{N} \mathbf{u}_i^n \psi_i(\mathbf{x},t) I_{[t_n,t_{n+1})}(t), \quad \mathbf{x}\in\Omega, \quad t\in[0,T] \tag{18}$$

Finally one should note that (17) contains two unknowns at the time level $n+1$, namely $\mathbf{u}_i^{n+1}$ and V_i^{n+1}. Thus, we need an additional equation for the volumes of particles. There are two alternative approaches to find V_i^{n+1}. One may apply numerical integration to compute V_i^{n+1} from definition (8), or one may obtain the additional equation for V_i^{n+1} by differentiating Equation (8) with respect to t, namely

$$\dot{V}_i(t) = \sum_{j\in N(i)} (\boldsymbol{\gamma}_{ij}\dot{\mathbf{x}}_j - \boldsymbol{\gamma}_{ji}\dot{\mathbf{x}}_i) \tag{19}$$

In practice we choose the first approach to compute the volumes V_i^{n+1}, although there is no advantage or disadvantage of one approach over the other one.

1.2. Some properties of the FVPM

As one can note from the previous derivation of the FVPM, this scheme is defined by the following factors: the position of the particles $\mathbf{x}_i$, the smoothing kernel W, the smoothing length h, the velocity of the particles $\mathbf{a}$ and the numerical flux function $\mathbf{g}$. Geometrical information about the particles and about their relative position is carried by the coefficients $\boldsymbol{\beta}_{ij}$. Therefore, they are also called *geometrical coefficients*. Only from formula (17), one would say that they play an important role in the scheme. Indeed, they have a significant influence on the properties of the method. Their heuristic interpretation (see e.g. [4]) shows the similarity between the FVPM and the classical finite-volume approach.

Therefore, before presenting the properties of scheme (15), we remember some important properties of the geometrical coefficients $\boldsymbol{\beta}_{ij}$.

Proposition 1
The coefficients $\boldsymbol{\beta}_{ij}$ satisfy

$$\boldsymbol{\beta}_{ij} = -\boldsymbol{\beta}_{ji} \quad \forall i,j = 1,\ldots,N \tag{20}$$

$$\boldsymbol{\beta}_{ij} = 0 \quad \text{if } \operatorname{supp}\psi_i \cap \operatorname{supp}\psi_j = \emptyset \tag{21}$$

$$\boldsymbol{\beta}_{ii} = 0 \quad \forall i = 1,\ldots,N \tag{22}$$

and

$$\sum_j \boldsymbol{\beta}_{ij} = \begin{cases} 0 & \text{if } \operatorname{supp}\psi_i \cap \partial\Omega = \emptyset \\ -\displaystyle\int_{\partial\Omega} \psi_i \mathbf{n}\,\mathrm{d}\sigma & \text{if } \operatorname{supp}\psi_i \cap \partial\Omega \neq \emptyset \end{cases} \tag{23}$$

Corollary 1
In the non-moving case, i.e. when $\dot{\mathbf{x}} = 0$, property (23) is sufficient to preserve constant states.

DOI: 10.1002/fld

Proofs of the above properties may be found in [9].

The properties of scheme (15) are mainly proved for the one-dimensional case and a scalar conservation law, such as a Lax–Wendroff-type consistency result in [2]. Monotonicity of the scheme, under a CFL-like condition, and an L^∞-stability for finite times of the approximate solution $\tilde{\mathbf{u}}$ was obtained in [8], also for one-dimensional scalar conservation laws. Only the conservativity of the method is proved in the general case.

Provided that the coefficients $\boldsymbol{\beta}_{ij}$ satisfy the skew symmetry condition (20) and that the numerical flux function $\mathbf{g}$ is conservative, scheme (15) is *conservative* in the sense of a classical FVM, i.e.

$$\frac{\mathrm{d}}{\mathrm{d}t}\left(\sum_{i=1}^{N} V_i \mathbf{u}_i\right) = -\int_{\partial\Omega} \mathscr{F}(\mathbf{u})\cdot\mathbf{n}\,\mathrm{d}\sigma \tag{24}$$

Here we wish to give an approximation property of the reconstruction formula (18) for a scalar conservation law on a two-dimensional domain $\Omega \subset R^2$. One may study in which sense, for example, u^0 is approximated by $\tilde{u}(\mathbf{x},0)=\sum_i u_i(0)\psi_i(\mathbf{x},0)$, where $u_i(0)$ are the local averages $1/V_i(0)\int u^0(\mathbf{x})\psi_i(\mathbf{x},0)\,\mathrm{d}\mathbf{x}$. A similar approximation result is also given in [2], but for another norm, $x\in R$ and for $u\in C_0^1(\mathbb{R}\times R^+)$. Here we apply the convergence results obtained by Babuska and Melenk in [12] for the partition of unity method (PUM).

Theorem 1 (*Approximation property*)
Let $\Omega\subset R^2$ be an open set, $\{\Omega_i\}$ be an open cover of Ω satisfying a pointwise overlap condition

$$\exists M\in\mathbb{N}:\forall \mathbf{x}\in\Omega,\quad \#\{i\,|\,x\in\Omega_i\}\leqslant M \tag{25}$$

and $\{\psi_i\}$ be a partition of unity subordinate to the cover $\{\Omega_i\}$, i.e. $\operatorname{supp}\psi_i\subset\bar{\Omega}_i, \forall i$, satisfying

$$\|\psi_i\|_{L^\infty}\leqslant C_\infty \tag{26}$$

where C_∞ is a constant. Let $u\in H^1(\Omega)$ be the function to be approximated and $u_i := 1/V_i\int_{\Omega_i} u(\mathbf{x})\psi_i(\mathbf{x})\,\mathrm{d}\mathbf{x}$ be the local averages, where $V_i=\int_{\Omega_i}\psi_i(\mathbf{x})\,\mathrm{d}\mathbf{x}$. Then $\tilde{u}(\mathbf{x}):=\sum_i u_i\psi_i(\mathbf{x})$ satisfies

$$\|u-\tilde{u}\|_{L^2(\Omega)}\leqslant MC_\infty^2 Ch\|\nabla u\|_{L^2(\Omega)} \tag{27}$$

where $h=\max_i\{\operatorname{diam}(\Omega_i)\}$ is a typical space scale called *smoothing length* and C is a constant independent of h.

Proof
The proof of this theorem follows very closely Reference [12]. First we state the following lemma. □

Lemma 1 (*Babuska and Melenk* [*12*])
Let Ω be an open set and $\{\Omega_i\}$ be an open cover of Ω satisfying the pointwise overlap condition (25). Let u, $u_i\in H^1(\Omega)$, be such that $\operatorname{supp}u_i\subset\overline{\Omega_i\cup\Omega}$. Then

$$\sum_i \|u\|^2_{L^2(\Omega_i)}\leqslant M\|u\|^2_{L^2(\Omega)} \tag{28}$$

$$\left\|\sum_i u_i\right\|^2_{L^2(\Omega)}\leqslant M\sum_i\|u_i\|^2_{L^2(\Omega_i)} \tag{29}$$

DOI: 10.1002/fld

Using the fact that $\sum_i \psi_i \equiv 1$ and formulas (26) and (29), we can express

$$\|u-\tilde{u}\|^2_{L^2(\Omega)} = \left\| \sum_i \psi_i (u-u_i) \right\|^2_{L^2(\Omega)} \leqslant M \sum_i \|\psi_i (u-u_i)\|^2_{L^2(\Omega_i)}$$

$$\leqslant M C^2_\infty \sum_i \|u-u_i\|^2_{L^2(\Omega_i)} \tag{30}$$

Now we need to estimate $\|u-u_i\|_{L^2(\Omega_i)}$. For this we use the following two lemmas that are similar to Lemmas 7.12 and 7.16 in [13].

Lemma 2
With the notations and under the assumptions from Theorem 1, we have

$$|u(x)-u_i| \leqslant \frac{C_\infty h^2}{2V_i} \int_{\Omega_i} \frac{1}{|x-y|} |\nabla u(y)| \, \mathrm{d}y \quad \text{a.e. on } \Omega_i \tag{31}$$

Proof
The proof of this lemma is very similar to that of Lemma 7.16 from [13], where $\psi_i \equiv 1$. □

Lemma 3 (*Gilbarg and Trudinger* [*13*])
Let $\mu \in (0,1)$ and V_μ be an operator on $L^1(\Omega)$ defined by

$$(V_\mu f)(x) = \int_\Omega |x-y|^{2(\mu-1)} f(y) \, \mathrm{d}y \tag{32}$$

The operator V_μ maps $L^p(\Omega)$ continuously into $L^q(\Omega)$ for any q, $1 \leqslant q \leqslant \infty$, satisfying $0 \leqslant \delta = \delta(p,q) = p^{-1} - q^{-1} < \mu$. Furthermore, for any $f \in L^p(\Omega)$,

$$\|V_\mu f\|_q \leqslant \left(\frac{1-\delta}{\mu-\delta} \right)^{1-\delta} (2\pi)^{1-\mu} |\Omega|^{\mu-\delta} \|f\|_p \tag{33}$$

Now, applying Lemma 3 with $f = |\nabla u| \in L^2(\Omega_i)$, since $u \in H^1(\Omega_i)$, $p=2$, $\mu = \frac{1}{2} \in (0,1)$, $q=2$ and, hence, $\delta = 0$, we obtain

$$\left\| \int_{\Omega_i} \frac{1}{|y-x|} |\nabla u(y)| \, \mathrm{d}y \right\|_{L^2(\Omega_i)} \leqslant 2\sqrt{2\pi} |\Omega_i|^{1/2} \|\nabla u\|_{L^2(\Omega_i)} \tag{34}$$

Using (31) and (34), we obtain

$$\|u-u_i\|_{L^2(\Omega_i)} \leqslant \frac{C_\infty h^2}{V_i} \sqrt{2\pi} h \|\nabla u\|_{L^2(\Omega_i)} \tag{35}$$

Moreover, from (30) we obtain

$$\|u-\tilde{u}\|^2_{L^2(\Omega)} \leqslant M C^2_\infty \sum_i C^2_\infty \left(\frac{h^2}{V_i} \right)^2 2\pi h^2 \|\nabla u\|^2_{L^2(\Omega_i)}$$

$$\leqslant M C^4_\infty C^2 h^2 \sum_i \|\nabla u\|^2_{L^2(\Omega_i)} \leqslant M^2 C^4_\infty C^2 h^2 \|\nabla u\|^2_{L^2(\Omega)}$$

DOI: 10.1002/fld

where we used (28) and the fact that $V_i = O(h^2)$. Thus, estimate (27) is obtained, which completes the proof of Theorem 1.

2. FVPM WITH MOVING BOUNDARIES

In the following we will formulate the method in the general case when the domain Ω depends on time, i.e. $\Omega = \Omega(t) \subset R^d$. Then a general discussion about how the particles may move in FVPM will be used further in Section 3.1. Here why a correction procedure for the computation of the geometrical coefficients is needed will be also explained and a simple correction procedure is proposed.

2.1. A modified FVPM on moving domains

When the domain Ω is moving, i.e. its shape is changing with time and thus Ω depends on time, i.e. $\Omega = \Omega(t)$, we have to take into account a contribution due to the moving boundary.

Let us assume that the boundary $\Gamma(t)$ of the domain $\Omega(t)$ is moving with a velocity $\mathbf{b}(\mathbf{x}, t)$, i.e. we can express

$$\Gamma(t) = \left\{ \mathbf{x}(t) | \mathbf{x}(t) = \mathbf{x}_0 + \int_0^t \mathbf{b}(\mathbf{x}(\tau), \tau)\, \mathrm{d}\tau, \mathbf{x}_0 \in \Gamma_0 \right\} \tag{36}$$

where Γ_0 is the initial boundary. Then, since the integration volume $\Omega(t)$ changes in time, in formula (6) there appears a new term:

$$\frac{\mathrm{d}}{\mathrm{d}t} \int_{\Omega(t)} \mathbf{u}\psi_i \, \mathrm{d}\mathbf{x} = \int_{\Omega(t)} \frac{\mathrm{d}}{\mathrm{d}t}(\mathbf{u}\psi_i)\, \mathrm{d}\mathbf{x} + \underbrace{\int_{\partial\Omega(t)} \psi_i \mathbf{u}\cdot\mathbf{b}\cdot\mathbf{n}\, \mathrm{d}\sigma}_{\text{the new term}}$$

$$= \int_{\Omega(t)} (\mathscr{F}(\mathbf{u}) \cdot \nabla\psi_i + \mathbf{u}\,\partial_t\psi_i)\, \mathrm{d}\mathbf{x} - \int_{\partial\Omega(t)} \psi_i (\mathscr{F}(\mathbf{u}) \underbrace{-\mathbf{u}\cdot\mathbf{b}}) \cdot \mathbf{n}\, \mathrm{d}\sigma$$

The derivation of the system of ODEs for $\mathbf{u}_i$ can be continued exactly like in Section 1.1 such that we obtain the following system:

$$\frac{\mathrm{d}}{\mathrm{d}t}(V_i \mathbf{u}_i) = -\sum_{j \in N(i)} |\boldsymbol{\beta}_{ij}| \mathbf{g}_{ij} - \int_{\partial\Omega(t)} \psi_i (\mathscr{F}(\mathbf{u}) - \mathbf{u}\cdot\mathbf{b}) \cdot \mathbf{n}\, \mathrm{d}\sigma \tag{37}$$

which differs from (12) only in the boundary term. Even Equation (19) for the volume $V_i(t)$ changes in this case to

$$\dot{V}_i(t) = \sum_{j \in N(i)} (\boldsymbol{\gamma}_{ij}\dot{\mathbf{x}}_j - \boldsymbol{\gamma}_{ji}\dot{\mathbf{x}}_i) + \int_{\partial\Omega(t)} \psi_i \mathbf{b}\cdot\mathbf{n}\, \mathrm{d}\sigma \tag{38}$$

However, one may still use Equation (8) for $V_i(t)$.

DOI: 10.1002/fld

2.2. How particles should move

In formula (37) there are two movements incorporated: **a**, the movement of the particles (through the numerical flux function **g**), and **b**, the movement of the boundary. Now we have to answer the question: given the velocity field **b**, how should the particles move?

In contrast to Lagrangian methods, e.g. the smoothed particle hydrodynamics (SPH) method [14], where particles are moved with the velocity of the fluid, in FVPM the particles are allowed to move along an almost arbitrary velocity field. Here we wish to exploit this advantage of FVPM, since there are cases when pure Lagrangian particles lead to severe difficulties, e.g. when solving problems where shocks are developed [7, 9]. Recognizing that shock waves are generic solutions of conservation laws, we are looking for non-Lagrangian particle motions.

As noted previously, in FVPM the particles should be moved in such a way that they always cover the domain. One may also imagine that the particles should be quite homogeneously distributed in the domain. Otherwise, when, at the same time, there are regions with very high and very low density of particles, the smoothing length h is either too small (and then holes are developed) or too large (and then some particles will have a high number of neighbours). In [7], where an adaptive smoothing length is used, it is shown that large variations in the smoothing length may lead to instabilities. Hence, beginning with homogeneously distributed particles, we wish to have a smoothly varying particle distribution.

Based on a two-dimensional test problem posed on a moving domain, a special Ansatz for the movement of the particles will be proposed.

2.3. A new correction procedure

Since the coefficients $\boldsymbol{\beta}_{ij}$ are given by integral quantities, see (14), one needs to introduce a numerical integration technique to compute the geometrical coefficients and this leads to additional errors, such that conditions (20)–(23) may not be satisfied exactly. However, the properties of the FVPM heavily rely on the conditions (20)–(23) of the $\boldsymbol{\beta}_{ij}$'s. Furthermore, if (23) is not exactly satisfied, then constant states will be no longer preserved (see Corollary 1).

Hence, applying a numerical quadrature to compute the geometrical coefficients requires in the sequel a correction procedure to ensure that the conditions (20)–(23) are satisfied exactly. See Section 3.2 or [4, 8, 9] for comparing numerical results obtained with and without correction procedures. First of all one should note that if one uses formula (14), then some properties of $\boldsymbol{\beta}_{ij}$'s still hold, such as $\boldsymbol{\beta}_{ii}=\mathbf{0}$, $\boldsymbol{\beta}_{ij}=-\boldsymbol{\beta}_{ji}$, and $\boldsymbol{\beta}_{ij}=\mathbf{0}$ for non-overlapping particles.

Let us discuss in the following how to ensure condition (23). The basic idea consists in firstly computing the coefficients $\tilde{\boldsymbol{\beta}}_{ij}$ by rough numerical integration in order to keep the computation costs as low as possible and then to modify them by an appropriate correction term $\bar{\boldsymbol{\beta}}_{ij}$.

A correction procedure given in [8], based on solving an undetermined linear system, works in general only for one-dimensional problems, since in multidimensional computations it is too expensive. A second approach, proposed by Keck [4], consists of a fast pairwise correction, where the defect of each particle is successively shifted to the 'next' neighbour while preserving conditions (20) and (23). For details refer to [4].

Here we will use the following alternative approach. Instead of correcting the coefficients $\tilde{\boldsymbol{\beta}}_{ij}$ obtained by a numerical quadrature, we add, for all interior particles i, the following term to the right-hand side of scheme (17):

$$-\Delta t\mathscr{G}(\mathbf{u}_i^n)\cdot\tilde{\boldsymbol{\beta}}_{ii}^n \tag{39}$$

DOI: 10.1002/fld

where $\tilde{\boldsymbol{\beta}}_{ii}^n := -\sum_j \tilde{\boldsymbol{\beta}}_{ij}^n$ is the defect for the particle i and $\mathscr{G}$ is the modified flux (13). Then scheme (17) becomes

$$V_i^{n+1}\mathbf{u}_i^{n+1} = V_i^n\mathbf{u}_i^n - \Delta t \sum_{j\in N(i)} |\tilde{\boldsymbol{\beta}}_{ij}^n|\mathbf{g}_{ij}^n - \Delta t\mathscr{G}(\mathbf{u}_i^n)\cdot\tilde{\boldsymbol{\beta}}_{ii}^n \tag{40}$$

Remember that $\mathbf{g}$ is a numerical flux function consistent with $\mathscr{G}$, i.e. $\mathbf{g}(t,\mathbf{x},\mathbf{u},\mathbf{x},\mathbf{u},\mathbf{n}) = \mathscr{G}(\mathbf{u})\cdot\mathbf{n}$. In this way, using scheme (40), the constant states are preserved in the non-moving case, even if $\sum_j \tilde{\boldsymbol{\beta}}_{ij} \neq 0$.

A disadvantage of this approach is that the conservativity of the scheme is lost by adding this correction term. Indeed, in general, one has

$$\sum_{i=1}^N V_i^{n+1}\mathbf{u}_i^{n+1} = \sum_{i=1}^N V_i^n\mathbf{u}_i^n - \Delta t\sum_{i=1}^N \mathscr{G}(\mathbf{u}_i^n)\cdot\tilde{\boldsymbol{\beta}}_{ii}^n \neq \sum_{i=1}^N V_i^n\mathbf{u}_i^n$$

Because the defect $\tilde{\boldsymbol{\beta}}_{ii}^n$ is of the order of the integration error, i.e.

$$|\tilde{\boldsymbol{\beta}}_{ii}^n| = \mathscr{O}(h^{s+d-1}) \tag{41}$$

where $s\geqslant 1$ is the order of the numerical quadrature used to compute $\tilde{\boldsymbol{\beta}}_{ij}^n$, we may express

$$\sum_{i=1}^N V_i^{n+1}\mathbf{u}_i^{n+1} = \sum_{i=1}^N V_i^n\mathbf{u}_i^n + \mathscr{O}(h^s)$$

assuming $\Delta t = \mathscr{O}(h)$, which follows from a typical CFL-type condition, as well as $N = \mathscr{O}(1/h^d)$. Despite the fact that scheme (40) is only approximately conservative, we will use this modified FVPM scheme in the numerical computations from Section 3.

3. NUMERICAL EXPERIMENTS

In this section we apply the FVPM scheme (40) to different test problems in order to validate the method.

To implement an FVPM scheme, one has to start by defining a set of particles in the domain. We are using uniform or non-uniform distributed and non-moving or moving particles. More precisely, the domain Ω is divided firstly into $N = nx\times ny$ rectangular cells of size $\Delta x\times\Delta y$, where nx and ny are the numbers of cells in the x- and y-directions, respectively. Then, if we wish to use uniform distributed particles, we take a particle i in the middle of the cell, otherwise we let it be randomly distributed within the cell and we call it a *quasi-random* particle distribution. Since we choose $\Delta y = \Delta x$, further on only Δx will appear. If and how particles are moved will be specified later in each example. The piecewise quadratic kernel (4) is used to obtain a two-dimensional partition of unity with a tensor product structure.

The next step is to compute the geometrical coefficients $\boldsymbol{\beta}_{ij}$ using (14). In the particular case of uniform distributed, non-moving particles and $h = \Delta x$, coefficients $\boldsymbol{\beta}_{ij}$ can be computed exactly [8, 9] and no correction procedure is needed. When using quasi-random particles, firstly we compute the intersection of the supports of pairwise interacting particles, and then a Gauss quadrature rule

DOI: 10.1002/fld

with 4×4 points is applied to compute $\boldsymbol{\beta}_{ij}$. When particles are moving in time, volumes V_i are computed in each time step from (8) by the same quadrature rule as used for computing $\boldsymbol{\beta}_{ij}$.

We use the numerical flux function of LeVeque [11] for computing the term $\mathbf{g}_{ij}$. The solution is reconstructed on a uniform grid of size $\Delta x\times\Delta x$ using formula (18).

3.1. A test problem with moving boundaries

We concentrate now on simulating a flow around an oscillating circle in a spatial two-dimensional geometry.

The computational domain is given by $\Omega(t)=[0,1]\times[0,1]\setminus B_{\mathrm{R}}(t)$, where $B_{\mathrm{R}}(t)=\{(x,y)\in\mathbb{R}^2:\|x-x_c(t),y-y_c(t)\|\leqslant R\}$ is the ball of center $(x_c(t),y_c(t))$ and radius R. Let us denote the domain's boundary by $\partial\Omega(t):=\Gamma_0\cup\Gamma_{\mathrm{R}}(t)$, where Γ_0 is the exterior boundary and $\Gamma_{\mathrm{R}}(t)$ is the boundary of the moving ball (see Figure 2).

We consider a simple, rigid movement of the ball, although one may consider another types of movements. In our example the ball is oscillating up and down, for example, with respect to the following equations:

$$\dot{x}_c(t)=0,\quad x_c(0)=x_c^0 \tag{42}$$

$$\dot{y}_c(t)=A\omega\cos(\omega t),\quad y_c(0)=y_c^0 \tag{43}$$

where A is *the amplitude of the motion* and ω is *the frequency*.

For the fluid–structure interaction problem that is considered here, the effects due to viscosity can be neglected. Hence, the fluid is modeled by Euler's equations for compressible inviscid flow [11] and is given by

$$\partial_t\mathbf{u}(\mathbf{x},t)+\nabla\cdot\mathscr{F}(\mathbf{u}(\mathbf{x},t))=0,\quad \mathbf{x}\in\Omega(t) \tag{44}$$

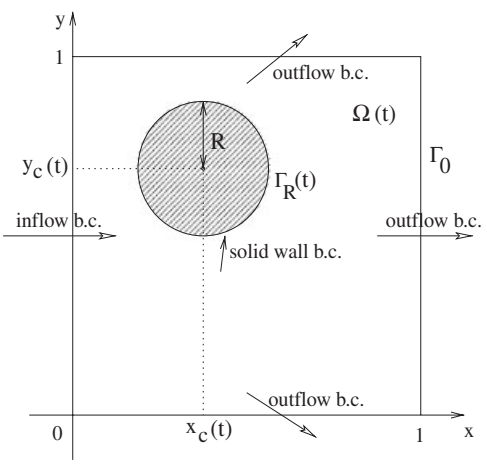

Figure 2. The computational domain of the test problem.

DOI: 10.1002/fld

where

$$\mathbf{u}=\begin{pmatrix}\rho\\ \rho u\\ \rho v\\ \rho E\end{pmatrix},\quad \mathbf{f_1}=\begin{pmatrix}\rho u\\ \rho u^2+p\\ \rho uv\\ u(\rho E+p)\end{pmatrix},\quad \mathbf{f_2}=\begin{pmatrix}\rho v\\ \rho uv\\ \rho v^2+p\\ v(\rho E+p)\end{pmatrix},\quad \mathscr{F}=(\mathbf{f_1},\mathbf{f_2})$$

ρ, u, v, E, and p denote the density, velocity in the x- and y-directions, total energy, and pressure, respectively. Equation (44) is closed by the equation of state for a perfect gas: $p=(\gamma-1)\rho(E-(u^2+v^2)/2)$, with $\gamma=1.4$.

Equation (44) is completed by the initial condition

$$\mathbf{u}(\mathbf{x},0)=\mathbf{u}_0(\mathbf{x})=\begin{pmatrix}\rho_0\\ \rho_0 u_0\\ \rho_0 v_0\\ \rho_0 E_0\end{pmatrix},\quad \mathbf{x}\in\Omega(t)$$

where $\rho_0=1$, $p_0=1$, $u_0=7/\gamma$, $v_0=0$ (corresponding to a supersonic inflow with $Ma=5$), and E_0 is computed from the equation of state, as well as the following boundary conditions:

- inflow boundary conditions on the left part of Γ_0;
- outflow boundary conditions on the rest of Γ_0;
- solid wall boundary conditions on the moving boundary $\Gamma_R(t)$.

Following the discussion from Section 2.2, we assume that the movement of the particles **a** is given by the solution to a Laplace equation with the following boundary conditions: namely *zero* velocity at the fixed boundary Γ_0 and the boundary velocity at the moving boundary $\Gamma_R(t)$:

$$\begin{aligned}\Delta\mathbf{a}(\mathbf{x},t)&=\mathbf{0}, \quad \Omega(t)\\ \mathbf{a}(\mathbf{x},t)&=\mathbf{0}, \quad \Gamma_0\\ \mathbf{a}(\mathbf{x},t)&=\mathbf{b}, \quad \Gamma_R(t)\end{aligned}\tag{45}$$

The boundary velocity **b** is given by the motion of the ball, i.e. $\mathbf{b}=(\dot{x}_c(t),\dot{y}_c(t))$, where $\dot{x}_c(t)$ and $\dot{y}_c(t)$ are given by (42) and (43), respectively.

In this way, the velocity field **a** will be smooth and the particles will follow the time-dependent computational domain, since particles near the boundary move with the boundary and do not get out of the domain, because the solution **a** satisfies a maximum principle.

Our approach is very similar to the arbitrary Lagrange–Euler method (ALE-method [15]) and the spring analogy method [16] used in mesh-based computations on a moving fluid domain. As in the FVPM, in the ALE method the coordinates are neither fixed (Eulerian) nor move with the fluid (Lagrangian), but they can move in an arbitrary way. When the boundary is displaced, the mesh is deformed and mesh cells are squeezed and stretched or maybe even inverted. The spring analogy is then used in [17] to restore the mesh to a more regular state. In our example, we may also imagine that the particles are linked between the boundaries through fictitious springs.

DOI: 10.1002/fld

Remark
In our example, since the movement of the boundary is restricted to a rigid body movement of an isolated object, the whole distribution of particles could be moved with the boundary. In this way, the particles remain rigid, i.e. there is no relative motion between the particles. The advantage of this rigid movement is clear: we do not have to recompute every time the coefficients $\boldsymbol{\beta}_{ij}$, for example. However, the rigid movement approach is less general than the one proposed here.

In [9] we have also investigated under which conditions on the motion of the circle and the smoothing length of the particles no 'holes' are developed in the domain. By a 'hole' we understand a space which is not covered by the support of any particle.

Now we present some numerical results concerning this test problem.

If the circle moves periodically up and down, such as specified in (42) and (43), there exists a periodic solution, i.e. after a few oscillations up and down the flow becomes periodic, with the same period as the circle's movement. To see this, we compute the difference between the solution every time when the circle attains its initial position, moving upwards, i.e. exactly after a complete period:

$$e_k = \sum_{i \in N} |\rho_i^k V_i^k - \rho_i^{k+1} V_i^{k+1}|, \quad k = 0, 1, \ldots, k_{\max}$$

where $k_{\max} = [T/P]$, $P = 2\pi/\omega$ is the period of the movement, T is the final time, t_0 is the time when the circle starts to move, $\rho_i^k = \rho_i(t_0 + kP)$, and $V_i^k = V_i(t_0 + kP)$. For this computation, we choose $N = 50 \times 50$ uniform distributed particles, $t_0 = 0$, $\omega = 10\pi$, $A = 0.1$, $P = 2\pi/\omega = 0.2$, and $T = 4.05$. Hence, $k_{\max} = 20$. As can be seen in Figure 3, after around 10 complete oscillations, the differences e_k are so small that the flow can be considered to be periodic.

Now we choose $N = 100 \times 100$ quasi-random distributed and moving particles. The movement of the circle is as before, i.e. $A = 0.1$ and $\omega = 10\pi$. The solution at time $T = 0.55$ is presented in Figures 4 and 5. In Figure 4(left) one may see the irregular particle positions together with their

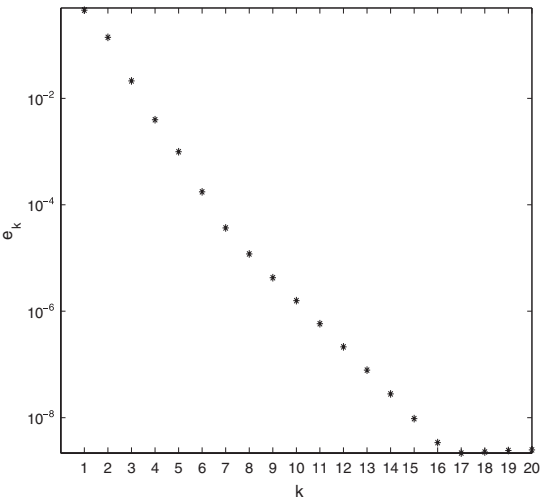

Figure 3. Differences e_k *versus* k.

DOI: 10.1002/fld

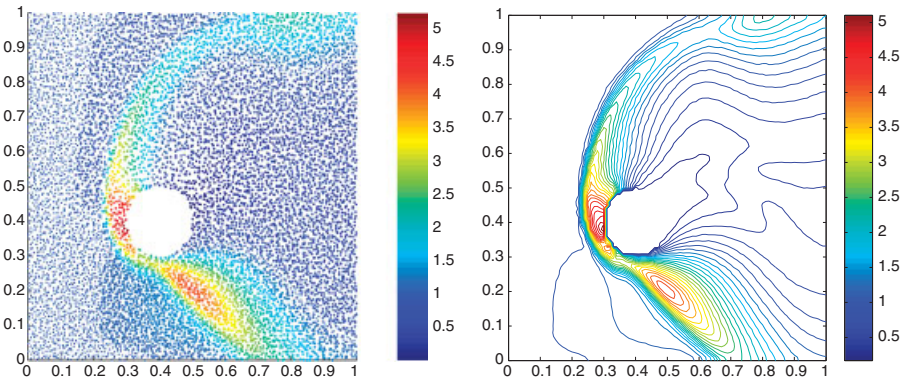

Figure 4. $N = 100 \times 100$ quasi-random distributed particles and their corresponding density (left) and isolines of the density (right).

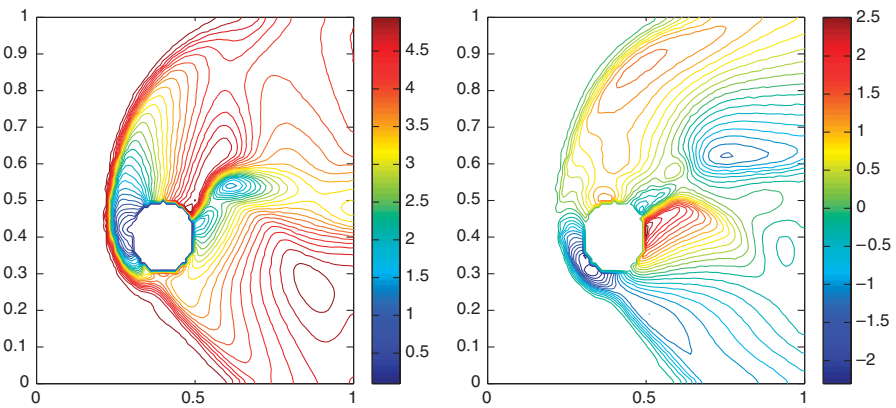

Figure 5. Isolines of u- (left) and v-velocity components (right) in the same case as in Figure 4.

corresponding density. The solution reconstructed on a uniform grid is shown in Figure 4(right) (isolines of the density) and Figure 5 (isolines of the velocity components). These results show that the method also works in the case of a time-dependent domain using irregular distributed and moving particles.

3.2. A shock tube problem

Here we apply the FVPM to the two-dimensional shock tube problem from inviscid gas dynamics governed by the Euler equations (44) with the following initial conditions:

$$\rho(x, y) = \begin{cases} \rho_{\mathrm{L}}, & x \leqslant 0.5 \\ \rho_{\mathrm{R}}, & x > 0.5 \end{cases}, \quad p(x, y) = \begin{cases} p_{\mathrm{L}}, & x \leqslant 0.5 \\ p_{\mathrm{R}}, & x > 0.5 \end{cases}$$

$$\mathbf{v}(x, y) = \mathbf{0}$$

DOI: 10.1002/fld

for $(x, y) \in [0, 1] \times [0, 1] \subset \mathbb{R}^2$, with parameters suggested by Sod [18]

$$\rho_L = 1, \quad \rho_R = 0.125, \quad p_L = 1, \quad p_R = 0.1$$

This problem can be realized experimentally by the sudden breakdown of a diaphragm in a long one-dimensional tube separating two initial gas states at different pressures and densities. If viscous effects can be neglected along the tube walls and if an infinitely long tube is considered, the exact solution to the one-dimensional Euler equations can be obtained on the basis of simple waves separating regions of uniform conditions [19].

We perform a two-dimensional computation for, in fact, a one-dimensional problem. We expect to obtain a quasi-one-dimensional solution to the two-dimensional Euler's equation (44), i.e. the solution should vary only in the x-direction.

The computations are done using $N = 100 \times 100$ or 500×500 uniformly or quasi-random distributed particles. The solution is computed at time $T = 0.15$. The coefficients $\boldsymbol{\beta}_{ij}$ are computed either exactly or approximately. In the first case, when $\boldsymbol{\beta}_{ij}$ are computed exactly, we are also using a layer of ghost cells such that no boundary approximations are made, since on the top and bottom we apply periodic boundary conditions and on the left and right parts we supply the constant states from the initial condition. This can be made as long as the shock or rarefaction wave does not reach the boundary, and this is not the case at $T = 0.15$. In the case when $\boldsymbol{\beta}_{ij}$ cannot be computed exactly, we apply the boundary treatment and the correction procedure explained before. On the top and bottom parts of the domain, we apply the solid wall boundary condition and on the left and right parts of the boundary we apply the outlet boundary condition. No particular measures are taken to keep the flow inside the tube one dimensional.

In Figure 6(left), we show the positions of 100×100 quasi-random distributed particles together with their corresponding densities. Then the solution is reconstructed on a 100×100 uniform grid, and isolines of the density are shown in Figure 6(right).

As mentioned in Section 1.2, if the coefficients $\boldsymbol{\beta}_{ij}$ are not corrected such that condition (23) is satisfied, the constant states are not preserved, as can be seen in Figures 7(left) and 8. Furthermore, we have also implemented the correction procedure proposed by Keck in [4], and isolines of the density are shown in Figure 7(right). After a rough comparison between the density obtained using

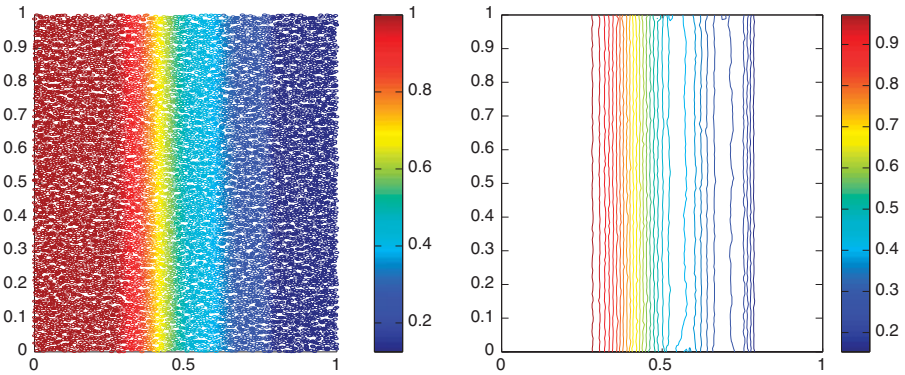

Figure 6. $N = 100 \times 100$ quasi-random particles and their corresponding density (left), with $h = 1.5\Delta x$, and isolines of the density reconstructed on a uniform grid (right), with our correction procedure.

DOI: 10.1002/fld

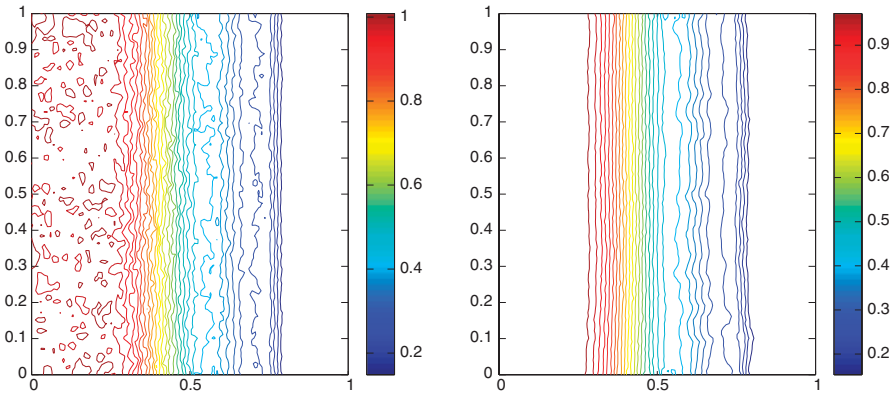

Figure 7. Isolines of the density reconstructed on a uniform grid without correcting the geometrical coefficients (left) and with Keck's correction procedure (right).

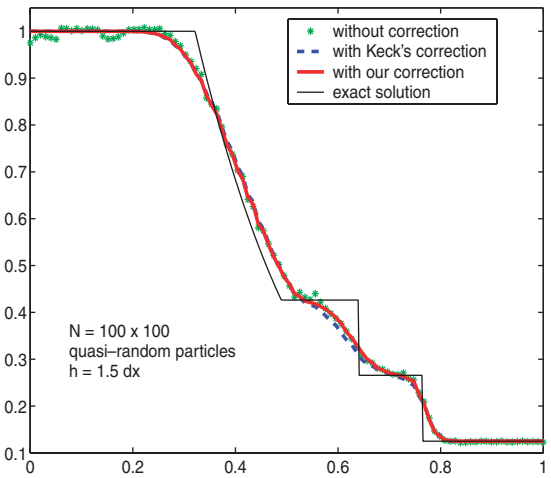

Figure 8. Cut in the x-direction at the middle of the domain, through the density profiles obtained in Figures 6(right), 7(left) and (right).

our and Keck's correction, see Figure 8, we conclude that the results are similar; therefore we will restrict in the following to our correction procedure.

In Figure 9 we compare the densities obtained with exact and computed coefficients $\boldsymbol{\beta}_{ij}$ in order to check the numerical approximation of the coefficients $\boldsymbol{\beta}_{ij}$. We used $N = 500 \times 500$ uniform distributed particles with $h = \Delta x$. As expected, the results are almost the same.

The influence of the smoothing length h on the solution is shown in Figure 10, where cuts through the density profile obtained for different h are shown. $N = 100 \times 100$ quasi-random distributed particles were used. As pointed out in [1] for Burgers' equation, the FVPM is quite robust when changing the smoothing length h. Decreasing the smoothing length yields a better resolution of the waves, without producing oscillations.

DOI: 10.1002/fld

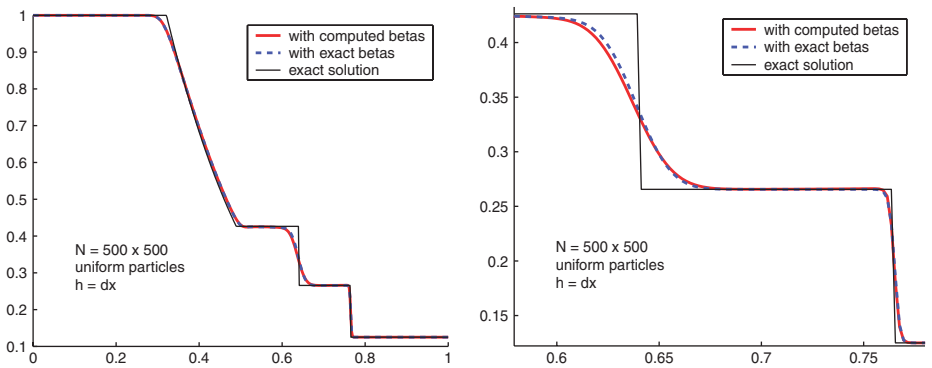

Figure 9. The density obtained with exact and with computed coefficients $\boldsymbol{\beta}_{ij}$ (left) and a zoomed view of the shock wave and the contact discontinuity (right).

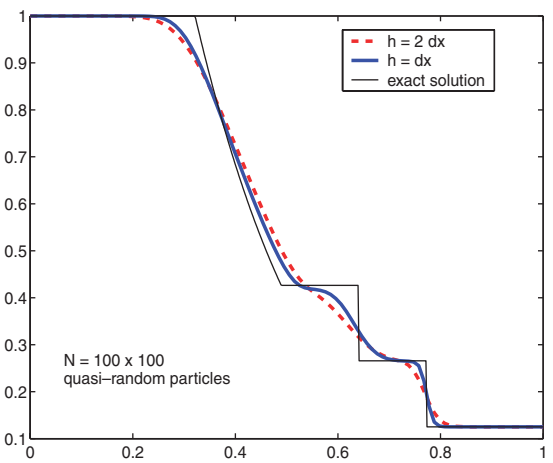

Figure 10. Influence of the smoothing length h on the density.

Finally, we compute numerical convergence rates in the discrete L_1- and L_2-norm for this problem. The error between the exact solution and the approximate solution is computed for a sequence of $N = 20\times 20,\ 40\times 40, \ldots, 320\times 320$ quasi-random distributed particles with different smoothing lengths h. In Table I the errors for the density together with the experimental order of convergence (EOC) computed from two meshes of size $N_1 = nx_1 \times nx_1$ and $N_2 = nx_2 \times nx_2$ as

$$\mathrm{EOC}_k = \log \frac{|\rho_{N_1} - \tilde{\rho}_{N_1}|_k}{|\rho_{N_2} - \tilde{\rho}_{N_2}|_k} \Bigg/ \log\left(\frac{nx_2}{nx_1}\right), \quad k = 1, 2 \tag{46}$$

are given. In Figure 11 we show the errors *versus* the number of points in one direction, in order to synthesize the results from Table I and for a better comparison. As expected, the numerical

DOI: 10.1002/fld

Table I. Discrete L_1- and L_2-errors of the density for the shock tube problem, for different h.

N	$h=\Delta x$	$\|\rho-\tilde{\rho}\|_1$	EOC_1	$\|\rho-\tilde{\rho}\|_2$	EOC_2
20×20	5.000000e−02	3.553001e−02		5.088527e−02	
40×40	2.500000e−02	2.603677e−02	0.4485	4.052730e−02	0.3284
80×80	1.250000e−02	1.723002e−02	0.5956	2.910075e−02	0.4778
160×160	6.250000e−03	1.120914e−02	0.6202	2.104956e−02	0.4673
320×320	3.125000e−03	7.298787e−03	0.6189	1.571074e−02	0.4220
N	$h=1.5\Delta x$	$\|\rho-\tilde{\rho}\|_1$	EOC_1	$\|\rho-\tilde{\rho}\|_2$	EOC_2
20×20	7.500000e−02	4.427848e−02		5.966602e−02	
40×40	3.750000e−02	3.029744e−02	0.5474	4.500231e−02	0.4069
80×80	1.875000e−02	2.056287e−02	0.5592	3.276041e−02	0.4580
160×160	9.375000e−03	1.368476e−02	0.5875	2.404254e−02	0.4464
320×320	4.687500e−03	9.053464e−03	0.5960	1.813783e−02	0.4066
N	$h=2\Delta x$	$\|\rho-\tilde{\rho}\|_1$	EOC_1	$\|\rho-\tilde{\rho}\|_2$	EOC_2
20×20	1.000000e−01	4.924631e−02		6.400495e−02	
40×40	5.000000e−02	3.534180e−02	0.4786	5.035410e−02	0.3461
80×80	2.500000e−02	2.460084e−02	0.5227	3.740869e−02	0.4287
160×160	1.250000e−02	1.666850e−02	0.5616	2.770045e−02	0.4335
320×320	6.250000e−03	1.110999e−02	0.5853	2.084552e−02	0.4102

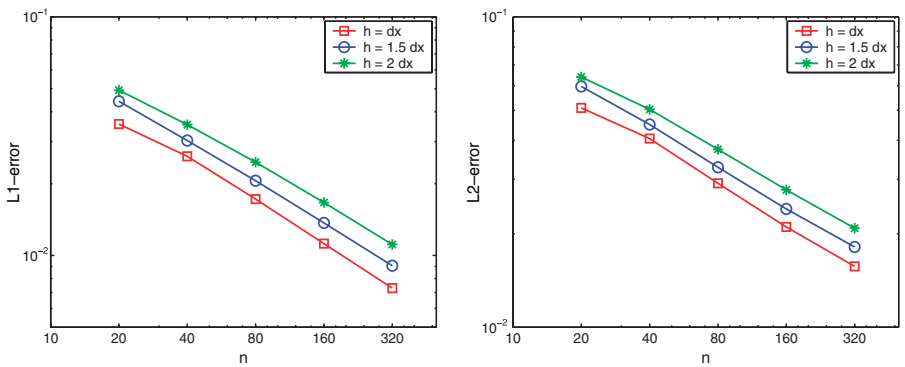

Figure 11. Discrete L_1-error (left) and L_2-error (right) of the density for the shock tube problem, at time $T=0.15$, using $N=n\times n$ quasi-random particles, for different h.

convergence rate does not depend on h. Furthermore, we remark that the error slightly increases with h. This is in agreement with the results obtained in Figure 10. However, in this case, the convergence rate does not approach the theoretical order one of convergence for smooth solutions. A similar convergence study, obtaining a similar convergence rate, is done in [1], also for the shock tube problem considered here, but the computations are one dimensional.

DOI: 10.1002/fld

3.3. A linear advection equation

Let us consider a simple linear equation in order to study further the numerical convergence of the FVPM, namely the following linear advection equation:

$$\partial_t u + \partial_x u = 0 \quad \text{on } [0,1]\times[0,1] \tag{47}$$

with a discontinuous initial condition

$$u_0(x,y) = \begin{cases} 1, & x \leqslant 0.5 \\ 0, & x > 0.5 \end{cases} \tag{48}$$

or with a smooth initial condition

$$u_0(x,y) = \exp\{-100((x-0.25)^2 + (y-0.25)^2)\} \tag{49}$$

The exact solution to Equation (47) is simply given by $u(x,y,t) = u_0(x-t,y)$.

The approximate solution is computed at $T = 0.25$, using $N = 80\times 80$ quasi-random distributed and non-moving particles with $h = 1.5\Delta x$. Outflow boundary conditions are used on all boundaries. In Figure 12, the solution to the linear advection equation (47) with the discontinuous initial condition (48), projected onto the u–x-plane, is shown. Then, in Figure 13, isolines of the exact solution and of the approximate solution of (47) with the smooth initial condition (49) can be found.

Finally, we compute numerical convergence rates in the discrete L_1- and L_2-norm for this linear problem, to see if we obtain better rates than in the non-linear case. The error between the exact solution and the approximate solution is computed for a sequence of $N = 20\times 20, 40\times 40, \ldots, 320\times 320$ quasi-random distributed particles, with different smoothing lengths h. In Tables II and III,

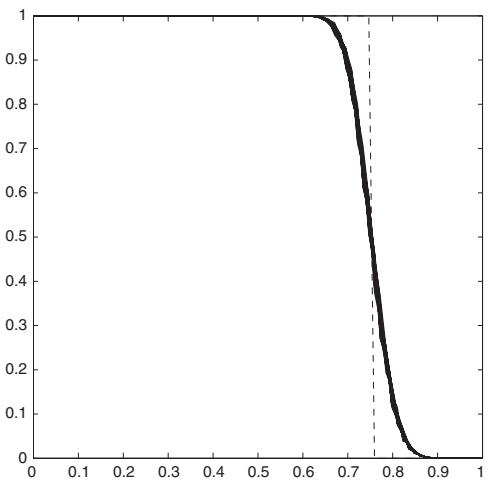

Figure 12. Solution to the linear advection equation with the discontinuous initial condition (48), projected onto the u–x-plane (the solid line) and the exact solution (the dotted line).

DOI: 10.1002/fld

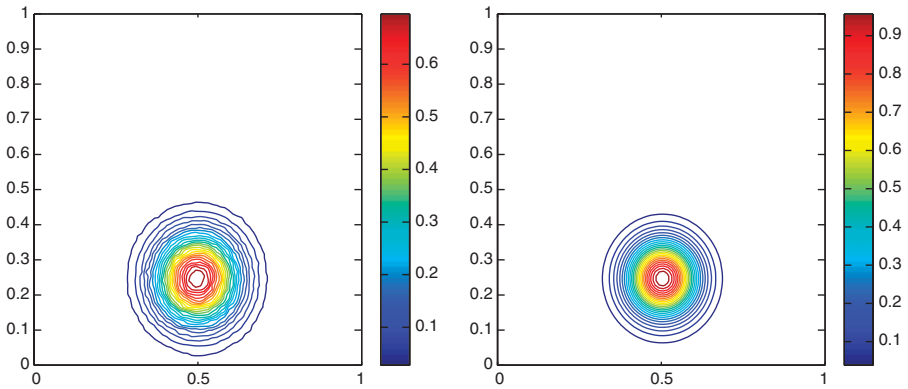

Figure 13. Isolines of the approximate solution (left) and of the exact solution (right) at $T = 0.25$, for the linear advection equation (47) with the smooth initial condition (49).

Table II. Discrete L_1- and L_2-errors for the linear advection equation with a discontinuous initial condition, for different h.

N	$h = \Delta x$	$\|u - \tilde{u}\|_1$	EOC_1	$\|u - \tilde{u}\|_2$	EOC_2
20×20	5.000000e−02	5.333467e−02		1.310182e−01	
40×40	2.500000e−02	3.603141e−02	0.5658	1.070453e−01	0.2915
80×80	1.250000e−02	2.419657e−02	0.5745	8.434356e−02	0.3439
160×160	6.250000e−03	1.738028e−02	0.4774	7.278524e−02	0.2126
320×320	3.125000e−03	1.227533e−02	0.5017	6.159035e−02	0.2409
N	$h = 1.5\Delta x$	$\|u - \tilde{u}\|_1$	EOC_1	$\|u - \tilde{u}\|_2$	EOC_2
20×20	7.500000e−02	7.515702e−02		1.524758e−01	
40×40	3.750000e−02	4.959395e−02	0.5997	1.208166e−01	0.3358
80×80	1.875000e−02	3.397842e−02	0.5455	9.962925e−02	0.2782
160×160	9.375000e−03	2.457986e−02	0.4671	8.771474e−02	0.1838
320×320	4.687500e−03	1.746742e−02	0.4928	7.491543e−02	0.2276
N	$h = 2\Delta x$	$\|u - \tilde{u}\|_1$	EOC_1	$\|u - \tilde{u}\|_2$	EOC_2
20×20	1.000000e−01	9.600310e−02		1.735468e−01	
40×40	5.000000e−02	6.332254e−02	0.6004	1.362808e−01	0.3487
80×80	2.500000e−02	4.349752e−02	0.5418	1.129455e−01	0.2710
160×160	1.250000e−02	3.128702e−02	0.4754	9.843819e−02	0.1983
320×320	6.250000e−03	2.221442e−02	0.4941	8.400084e−02	0.2288

the errors in the case of the jump solution and of the smooth solution, together with the EOC computed from (46), are given. In Figure 14 we show the errors *versus* the number of points in one direction in order to synthesize the results from Tables II and III and for a better comparison. As expected, the numerical convergence rate does not depend on h. Our results show an EOC which is less than the expected first-order convergence in the case of the smooth solutions.

DOI: 10.1002/fld

Table III. Discrete L_1- and L_2-errors for the linear advection equation with a smooth initial condition, for different h.

N	$h=\Delta x$	$\|u-\tilde{u}\|_1$	EOC_1	$\|u-\tilde{u}\|_2$	EOC_2
20×20	5.000000e−02	1.747204e−02		5.529881e−02	
40×40	2.500000e−02	9.979376e−03	0.8080	3.382673e−02	0.7091
80×80	1.250000e−02	5.163706e−03	0.9505	1.808657e−02	0.9032
160×160	6.250000e−03	2.772294e−03	0.8973	1.011878e−02	0.8379
320×320	3.125000e−03	1.594091e−03	0.7983	5.705053e−03	0.8267
N	$h=1.5\Delta x$	$\|u-\tilde{u}\|_1$	EOC_1	$\|u-\tilde{u}\|_2$	EOC_2
20×20	7.500000e−02	2.287496e−02		6.967677e−02	
40×40	3.750000e−02	1.353946e−02	0.7566	4.515581e−02	0.6258
80×80	1.875000e−02	7.793727e−03	0.7968	2.727371e−02	0.7274
160×160	9.375000e−03	4.302940e−03	0.8570	1.544056e−02	0.8208
320×320	4.687500e−03	2.610491e−03	0.7210	9.359223e−03	0.7223
N	$h=2\Delta x$	$\|u-\tilde{u}\|_1$	EOC_1	$\|u-\tilde{u}\|_2$	EOC_2
20×20	1.000000e−01	2.834719e−02		8.127777e−02	
40×40	5.000000e−02	1.769121e−02	0.6802	5.676342e−02	0.5179
80×80	2.500000e−02	1.043911e−02	0.7610	3.569118e−02	0.6694
160×160	1.250000e−02	5.926685e−03	0.8167	2.104068e−02	0.7624
320×320	6.250000e−03	3.485152e−03	0.7660	1.262132e−02	0.7373

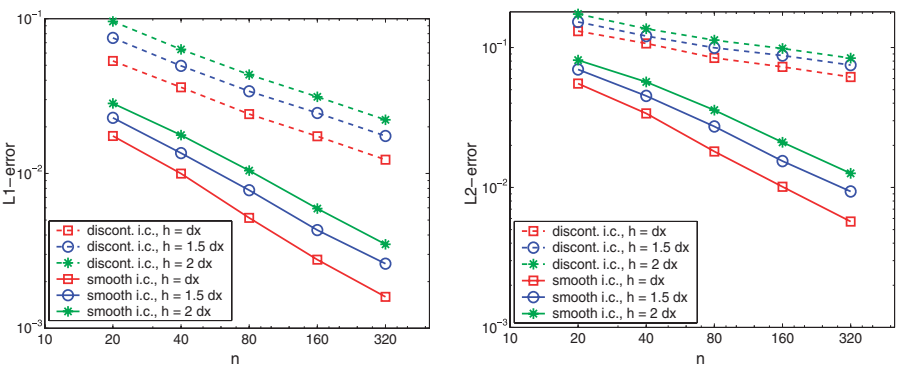

Figure 14. Discrete L_1-error (left) and L_2-error (right) for the linear advection equation with smooth and discontinuous initial conditions at time $T=0.25$, using $N=n\times n$ quasi-random particles, for different h.

4. CONCLUSIONS

In this paper we have further investigated the FVPM from a numerical and theoretical point of view. We derived the FVPM for a system of conservation laws in a bounded and time-dependent domain $\Omega(t)\subset\mathbb{R}^d$. Then we proved an approximation property of the reconstruction formula used in the FVPM, namely the fact that the reconstruction formula is only of order one. Also a new correction procedure, although only approximately conservative, was proposed.

DOI: 10.1002/fld

Furthermore, we presented here an application of the FVPM to a spatial two-dimensional problem posed on a moving domain, where the meshless character of the method is exploited. The particles are irregularly distributed in the domain and they are moving in a non-Lagrangian way such that they smoothly follow the time-dependent computational domain. Numerical results indicate that the method is well suited for such problems. Also the discretization of the boundary conditions works very satisfactory. Thus, a first step to applying the FVPM to real fluid–structure interaction problems, which in general limit the use of grid-based methods, is done. Finally, a convergence study for a shock tube problem and a simple linear advection equation was done.

ACKNOWLEDGEMENTS

This work has been supported by a DFG-Stipendium in the Graduiertenkolleg 431 at the University of Hamburg.

REFERENCES

1. Hietel D, Steiner K, Struckmeier J. A finite-volume particle method for compressible flows. *Mathematical Models and Methods in Applied Sciences* 2000; **10**(9):1363–1382.
2. Junk M, Struckmeier J. Consistency analysis of mesh-free methods for conservation laws. *GAMM-Mitteilungen* 2001; **2**:96–126.
3. Junk M. Do finite volume methods need a mesh? *International Workshop on Meshfree Methods for PDE*, Bonn, 2001.
4. Keck R. The finite volume particle method: a meshless projection method for incompressible flow. *Ph.D. Thesis*, University of Kaiserslautern. Shaker Verlag: Germany, 2002.
5. Keck R, Hietel D. A projection technique for incompressible flow in the meshless finite volume particle method. *Advances in Computational Mathematics* 2005; **23**(1–2):143–169.
6. Lamichhane BH. The applications of finite-volume particle method for moving boundary. *Master Thesis*, Department of Mathematics, University of Kaiserslautern, 2001.
7. Schick C. Adaptivity for particle methods in fluid dynamics. *Diploma Thesis*, Department of Mathematics, University of Kaiserslautern, 2000.
8. Teleaga D. Numerical studies of a finite-volume particle method for conservation laws. *Master Thesis*, Department of Mathematics, University of Kaiserslautern, 2000. (Available from: http://www.mathematik.tu-darmstadt.de/~dteleaga/MasterThesis.ps.)
9. Teleaga D. *A Finite-Volume Particle Method for Conservation Laws*. Logos Verlag: Berlin, 2005.
10. Yang Z. Efficient calculation of geometric parameters in finite-volume particle method. *Master Thesis*, Department of Mathematics, University of Kaiserslautern, 2001.
11. LeVeque RJ. *Finite Volume Methods for Hyperbolic Problems*. Cambridge University Press: Cambridge, 2002.
12. Babuska I, Melenk JM. The partition of unity method. *International Journal for Numerical Methods in Engineering* 1997; **40**:727–758.
13. Gilbarg D, Trudinger NS. *Elliptic Partial Differential Equations of Second Order*. Springer: Berlin, 1998.
14. Monaghan J. Smoothed particle hydrodynamics. *Annual Review of Astronomy and Astrophysics* 1992; **30**:543–574.
15. Donea J, Guiliani S, Halleux JP. An arbitrary Lagrangian–Eulerian finite element method for transient dynamic fluid–structure interactions. *Computer Methods in Applied Mechanics and Engineering* 1982; **33**:689–723.
16. Batina JT. Unsteady Euler airfoil solutions using unstructured dynamic meshes. *AIAA Journal* 1990; **28**(8): 1381–1388.
17. Blom F, Leyland P. Analysis of fluid–structure interaction on moving airfoils by means of dynamic unstructured meshes. *Proceedings of the 4th International Symposium on Fluid–Structure Interaction, Aeroelasticity, Flow-Induced Vibrations and Noise*, vol. I. ASME: New York, 1997.
18. Sod GA. A survey of several finite difference methods for systems of nonlinear hyperbolic conservation laws. *Journal of Computational Physics* 1978; **27**:1–31.
19. Hirsch C. *Numerical Computation of Internal and External Flows*, vol. 2. Wiley: New York, 1988.

DOI: 10.1002/fld